Ductile fatigue crack propagation in polycarbonate

N. Haddaoui, A. Chudnovsky and A. Moet
Department of Macromolecular Science, Case Western Reserve University, Cleveland, Ohio 44106, USA
(Received 8 October 1985)

Crack growth in thin polycarbonate sheets under cyclic loading is accompanied by a large zone of transformed (yielded) material. The homogeneous material transformation consumes energy and thus controls the rate of crack growth. The zone of transformed material deforms (i.e. expands and changes shape) with crack extension. A formalism for ductile fracture propagation analysis, based on the crack layer (CL) theory, is presented. This formalism relates kinetics of crack growth to the observed fracture mechanisms. In particular, resistance to crack propagation (toughness) is characterized by the product of the specific enthalpy of transformation γ^* and the resistance moment R_1 representing the magnitude of material transformation accompanying crack growth. According to the CL theory, γ^* is a material parameter which is found to be about 15 cal g^{-1}.

(Keywords: polycarbonate; ductile fracture; fatigue; crack propagation; specific enthalpy of damage; crack layer; energy release rate)

INTRODUCTION

Recent investigations reveal that fatigue crack propagation (FCP) in polycarbonate (PC) is affected by the molecular weight of the polymer[1,2], thickness of the specimen[1-3], temperature[2-4] and to a lesser extent by the test frequency[5,6].

Although polycarbonate is generally known as a ductile polymer, brittle fracture is frequently observed, and a brittle to ductile transition is shown to depend on the thickness, rate of loading[7] and the geometry of the notch[3].

In recent years, kinetics and mechanisms of fatigue crack growth in polycarbonate have been the focus of extensive research. However, little attention has been paid to relating the two.

In ductile fracture, the crack is usually surrounded by a zone of transformed (yielded material)[3,8-10]. The shape and size of the transformed zone are determined by the geometry of the notch and the loading level[3,11]. The material transformation within this zone consumes energy and thus constitutes the major source of resistance to crack growth. In this paper a systematic characterization of both the kinetics and mechanisms of fatigue crack propagation in thin polycarbonate sheets is presented. On the basis of the crack layer (CL) theory[12,13], a formalism that relates the two is proposed. This formalism constitutes a basic framework for general ductile fracture analysis.

EXPERIMENTAL

Compression moulded sheets of Bisphenol A-Polycarbonate (with a $MFI = 2$–3) supplied by Dow Chemical Company were used throughout this study. Standard tensile bars tested under monotonic tensile loading at a strain rate ($\dot{\varepsilon}$) of 0.02%s^{-1} display an elastic modulus (E) of 2.0 GPa, a yield stress of (σ_y) of 70 MPa and a failure stress (σ_F) of 67 MPa at an ultimate elongation of 36% over 60 mm gauge length.

Single edge notched (SEN) fatigue specimens are milled at very low speed to the dimensions 120 × 20 × 0.33 mm. The distance between grips is 80 mm. A 60° 'V' notch of 1 mm depth is introduced at the middle of one edge of the specimens.

Fatigue tests are conducted in a laboratory atmosphere on an MTS-800 machine using a sinusoidal waveform at a frequency of 0.5 Hz. The loading is tension–tension with a maximum stress of 33 MPa and a minimum to maximum load ratio $R = 0.4$. The crack and the surrounding damage are followed visually using a travelling optical microscope attached to a video camera assembly equipped with a visual display unit from which the entire history of crack propagation is recorded. Post fracture optical observations are carried out on a Zeiss light microscope.

RESULTS AND DATA ANALYSIS

Ductile FCP mechanism

Figure 1 is an optical micrograph taken under transmitted light of a side view of a specimen. It shows the typical pattern of crack propagation in thin sheets of polycarbonate. As can be seen, a zone of damaged (yielded) material precedes and surrounds the crack. The crack and the associated damage constitute a crack layer (CL). This CL morphology is reminiscent of that observed by several authors[3,8-10]. Furthermore, when the crack is relatively well developed, one notices pairs of shear bands within the CL at the tip of the main crack. Discontinuous fatigue crack propagation through shear bands has been reported in polycarbonate[14,15]. The region between the dark 'boundaries' of the CL ahead of the crack tip (*Figure 1*) seems to be covered by craze-like entities as shown in *Figure 2*. The average length of these entities is in the

0032-3861/86/091377$03.00

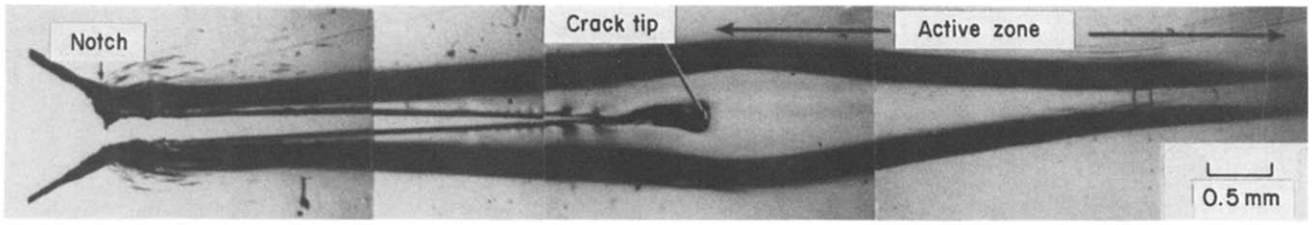

Figure 1 Composite optical micrograph of a side view of a well developed CL during stable crack growth

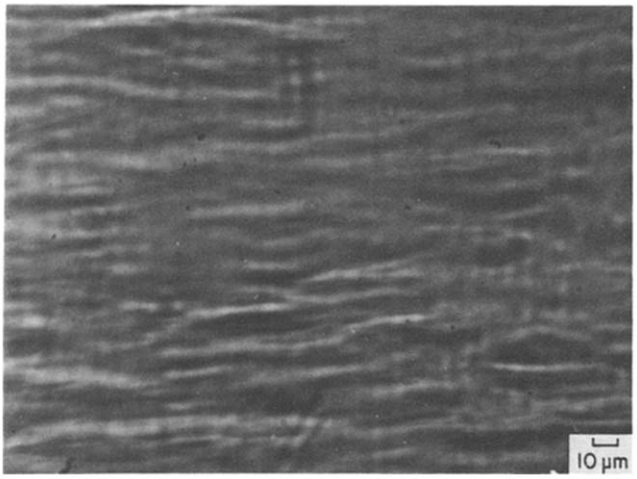

Figure 2 Transmission optical micrograph of a portion of the region between the dark 'boundaries' of the CL ahead of the crack tip showing craze-like entities

range of 40–70 μm with an average width of nearly 3 μm. Similar features, believed to be crazes, have been reported in polycarbonate under fatigue loading[16]. Once the crack passes such craze-like features, they could no longer be observed. Seemingly, these craze-like features appear to have been 'consumed' by further yielding (thinning) of the material immediately prior to cracking.

A cross section of the damage zone showing the thinning profile in the direction perpendicular to the crack path is exhibited in *Figure 3*. As can be noted, maximum thinning amounts to 50% of the initial thickness. Such thinning has been observed previously[9]. To investigate the extent of thinning in the deformed region, a specimen was fatigued under the conditions specified earlier in the Experimental section. When the crack tip reached point A, (*Figure 4*), the specimen was unloaded and, while still between grips, was immersed into liquid nitrogen for several hours. The specimen, still immersed in liquid nitrogen, was fractured under monotonically increasing load. The specimen thickness was measured along the crack path to determine the extent of thinning ahead of the crack. The results are shown in *Figure 5*. One can notice that beyond the deformed region delimited by the point B, there is no noticeable thinning, but there is a drastic decrease in thickness of as much as 50% of the original thickness in the vicinity of the crack tip. This fact indicates that the crack propagates through a zone of thinned material. The kink in the thickness profile observed at the crack tip is believed to be due to hydrostatic compressive stresses within the plane of loading while the crack was arrested prior to its critical (uncontrolled) propagation.

A composite optical micrograph (*Figure 6*) of the two halves of a broken specimen was taken under transmitted light. The crack and the surrounding yielded material

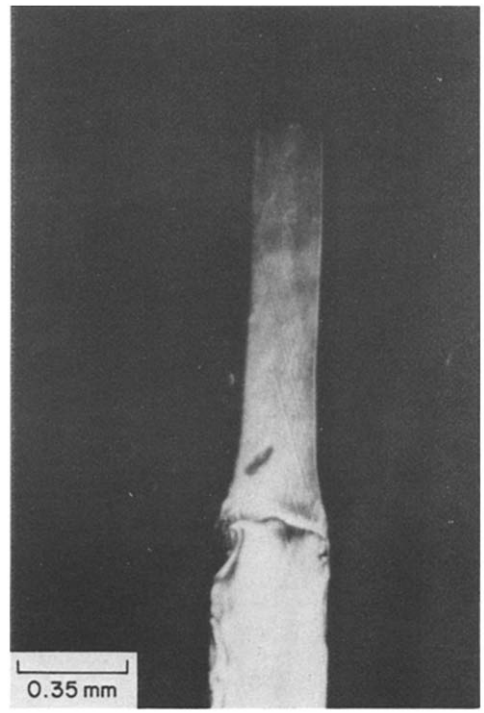

Figure 3 Optical micrograph of a transverse section showing the extent of thinning in the direction perpendicular to the crack path

propagate, as shown in *Figure 1*, until the leading edge of the deformation zone reaches point C; then ultimate failure takes place. The maximum width of the deformed region corresponds to the critical crack length indicated by l_c.

A typical thickness profile measured from the fatigue fracture surface throughout the width of the specimen is depicted in *Figure 7*. The thinning pattern resembles that observed in the crack arrest experiment (*Figure 5*). The majority of thinning corresponds to short crack length (up to 2 mm) at which thinning levels out. A hump in the thickness profile (vertical arrow) corresponds to the critical crack length and resembles that observed upon crack arrest (arrow A in *Figure 5*). Constant thinning of the specimen is also observed in the region of uncontrolled (unstable) propagation. *Figures 8a* and *8b* are typical reflected light micrographs of the fracture surface showing discontinuous crack propagation bands. *Figure 8a* corresponds to a short crack ($\sim$2 mm) where crack excursions are much smaller than those occurring at a longer crack (*Figure 8b*).

Kinetics of crack layer propagation

A schematic diagram representing the observed CL pattern (*Figure 1*) is shown in *Figure 9*. The region in front of the crack tip where progressive transformation (thinning) takes place is identified as the active zone. It is delimited by its leading and trailing edges.

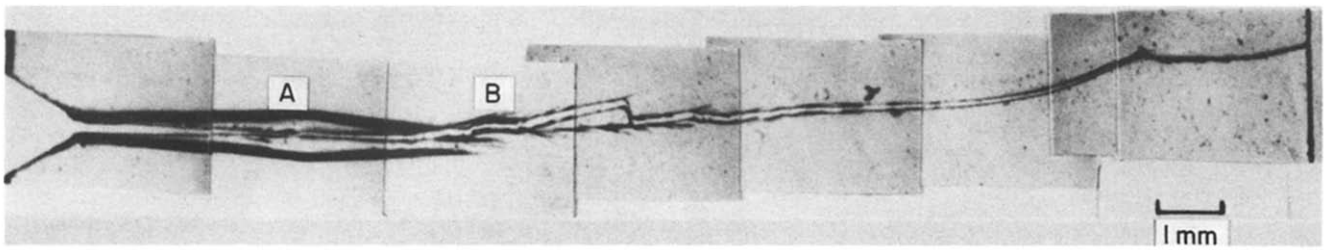

Figure 4 Composite transmission light micrograph of the two halves of a specimen fractured in liquid nitrogen. Point A indicates the tip of the fatigue crack and B indicates the corresponding leading edge of the active zone.

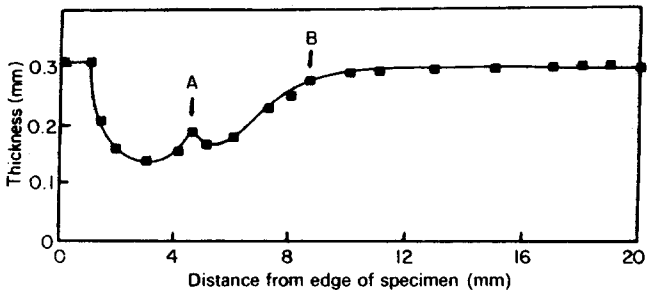

Figure 5 Extent of thinning along the crack path of the specimen shown in *Figure 4*

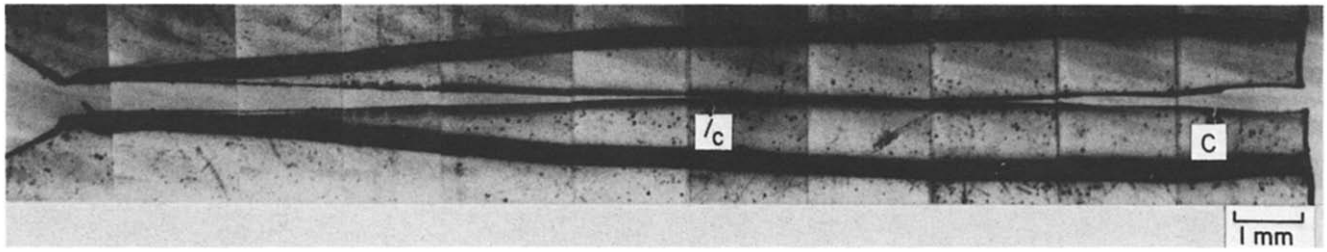

Figure 6 Composite optical micrograph of a side view of the two halves of a fractured specimen placed together after complete failure showing the increase of the width of transformed material with the crack length. Maximum width occurs at the critical crack length l_c. Point C indicates the position of the leading edge before final fracture

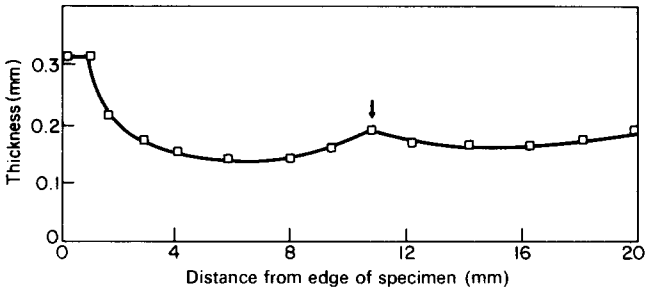

Figure 7 Extent of thinning along the fracture path of the specimen shown in *Figure 6*. Notice that constant thinning still takes place during unstable crack propagation

Evolution of the active zone constituting CL propagation is shown in *Figure 10*. Selected CL configurations are presented. These are traced from video play backs of crack propagation. The vertical scale in *Figure 10* is enlarged to elucidate the active zone evolution. The last active zone trace corresponds to the critical state immediately prior to ultimate failure. From *Figures 3*, *7* and *10* it is clear that the amount of material transformation and consequently energy absorption associated with CL propagation increase with crack length.

The simultaneous increases in length and width of the active zone (*Figure 11a*) indicates that expansion of the active zone is taking place concurrently with its translation. Changes of the aspect ratio (w/l_a) in a way are a measure of the distortion (shape changes) of the active zone. A constant width to length ratio would imply no

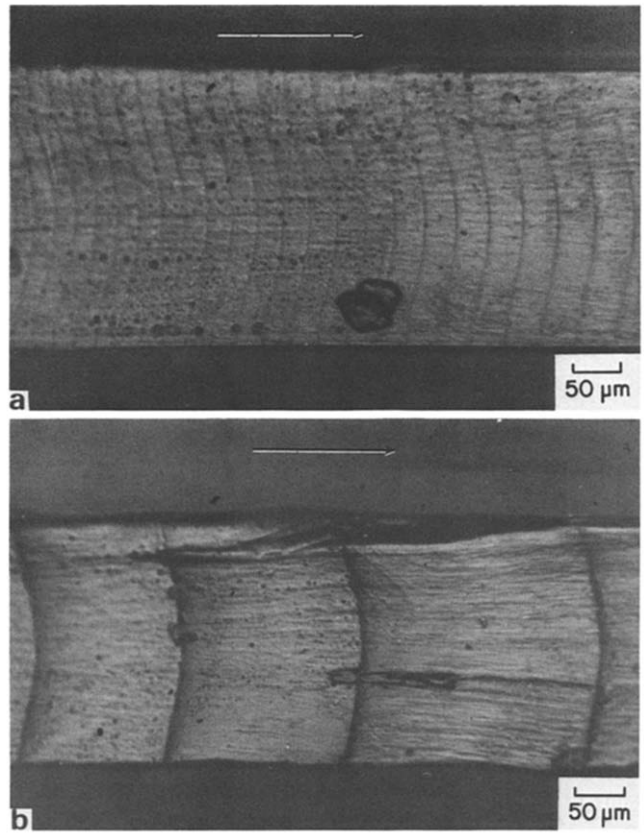

Figure 8 Reflected light micrographs of portions of the fracture surface showing discontinuous crack propagation bands at crack lengths of: (a) 2 mm and (b) 7 mm. The horizontal arrows indicate the direction of crack propagation

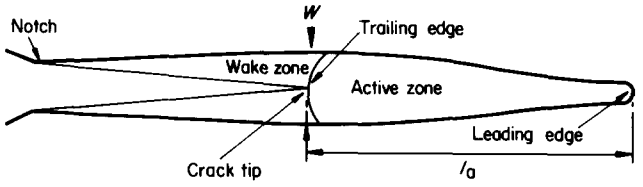

Figure 9 Schematic diagram of a CL and its main components

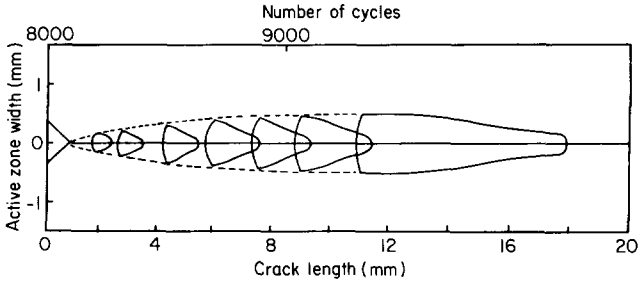

Figure 10 Evolution of the active zone during stable crack growth. The centre line represents the crack propagation path

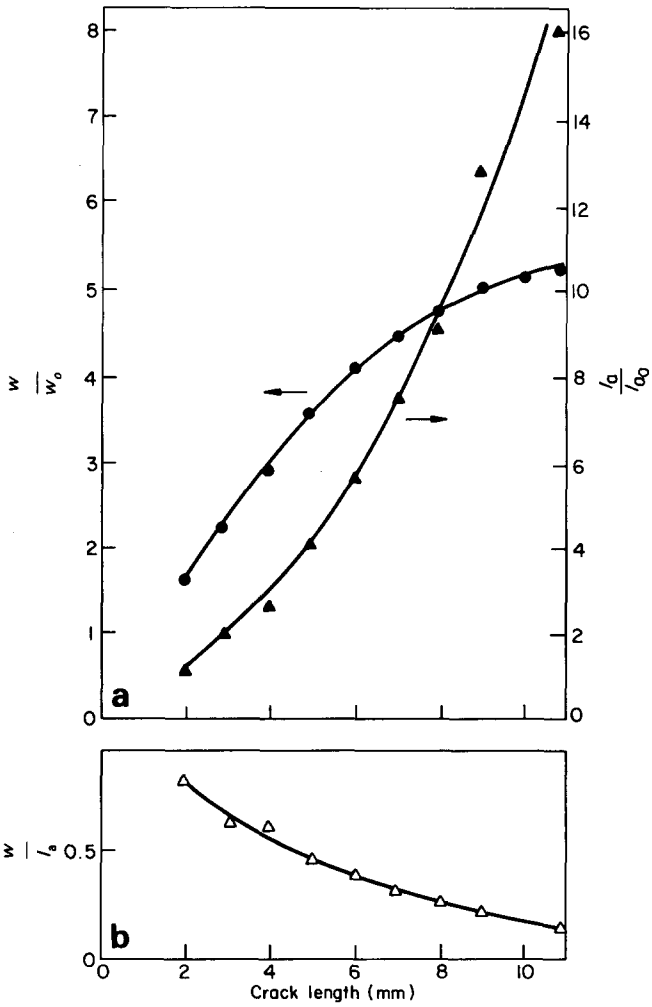

Figure 11 (a) Evolution of the active zone width (w) and active zone length (l_a). (b) Aspect ratio of the active zone with respect to the crack length

shape changes. *Figure 11b* shows that the deviation of the aspect ratio from constancy is appreciable. The active zone becomes more pointed as the crack advances.

Energy release rate evaluation

Since the active zone is comparatively large with respect to the specimen width and to the crack length, elastic solution of the energy release rate is no longer applicable. Elastoplastic solutions known to us predict plastic zones with shapes and sizes which are essentially different from the observed active zone (*Figures 1, 10*).

Therefore, the actual energy release rate was measured using conventional techniques based on the evolution of load–displacement curve[17]. Load–displacement curves during loading and unloading for a specimen with a specific crack length are recorded. The specimen subsequently is fatigued under conditions specified in the Experimental section until a prescribed crack increment is reached. For instance, load–displacement curves for $l = 6.5$ mm and $l = 8$ mm are shown in *Figure 12*. The area between the two loading curves (shadowed by horizontal lines) represents the change in the total potential energy (ΔP) associated with crack increment from 6.5 mm to 8 mm. The ratio $-\Delta P/\Delta l$ is conventionally considered equal to the energy release rate corresponding to an intermediate crack length ($l = 7.25$ mm). Since undetected crack propagation may occur during loading, the area between the unloading curves (shadowed by vertical lines) is a more reliable presentation of elastic potential energy change. A sequence of such load–displacement curves for our experiment is shown in *Figure 13*. The number at the top of each curve indicates the corresponding crack length in mm.

The *total* energy release rate A_1 based on the above procedure is plotted as a function of crack length in *Figure 14*. A_1 represents the potential energy change due to crack advance and simultaneous active zone movements. The vertical arrow points to the critical crack length, from which a critical energy release rate A_{1c} has been estimated. The dashed curve shows the conventional energy release rate G calculated on the basis of Irwin's plastic zone

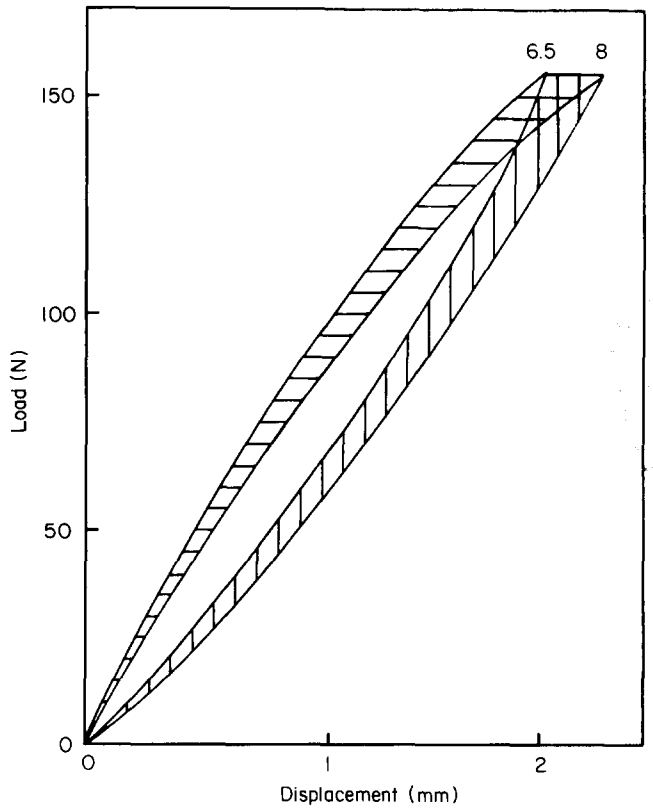

Figure 12 Load–displacement curves during the loading and unloading cycle for 6.5 and 8 mm crack lengths. The areas between the loading curves and unloading curves are essentially the same

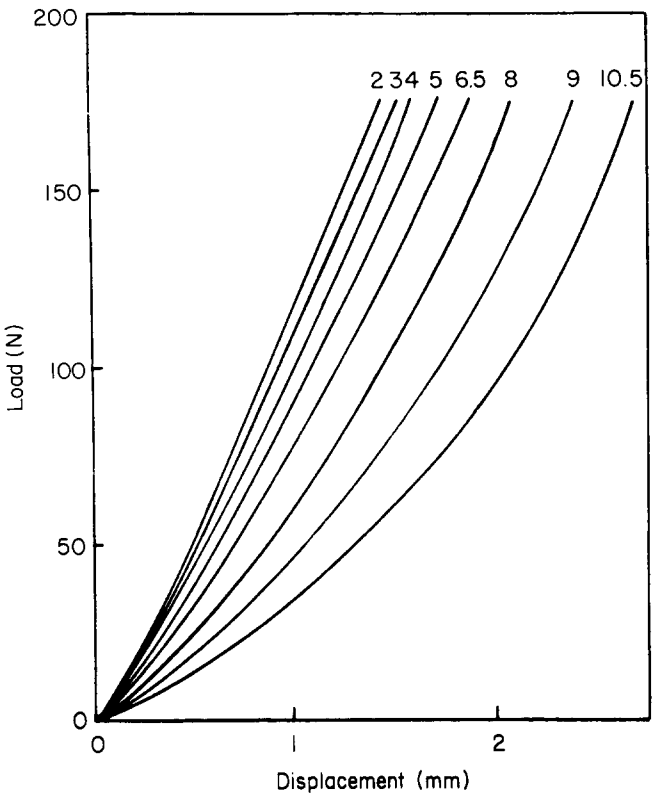

Figure 13 Load–displacement curves during the unloading process for different crack lengths. The number at the top of each curve indicates the corresponding crack length in mm

correction[18]. Recorded active zone length l_a is taken as the plastic zone size for G calculations.

Obviously, the Irwin elastoplastic G provides a good approximation to the total energy release rate up to a crack length of about 6–7 mm, i.e. ~0.3 of the specimen width. Above this range, the calculated energy release rate drastically departs from the measured values. A similar conclusion has been reached from the application of the Dugdale model to photoelastic analysis of ductile crack propagation in PC[9].

DISCUSSION

The evidence presented demonstrates that fatigue fracture in thin PC sheets occurs as active zone evolution (*Figure 10*). Evolution of the active zone involves three elementary movements: translation, expansion and distortion. Crack extension, causing ultimate separation of the specimen, coincides with active zone translation. The law of active zone translation, i.e. crack propagation, is derived as[12,13]

$$\frac{dl}{dN}=\frac{dD/dN}{\gamma^*R_1-A_1} \qquad (1)$$

where dl/dN is the average crack extension per cycle, D is the energy expended on material transformation associated with active zone evolution, γ^* is the specific enthalpy of damage (material transformation), R_1 is the translational resistance moment and A_1 is the total energy release rate. The nature of the three types of energy involved, i.e. γ^*R_1, A_1 and D, is further discussed below.

Evolution of $\gamma^*R_1-A_1$

Microscopic analysis (*Figures 1–7*) indicates that 'damage' in this particular case appears as homogeneous material transformation (yielding); therefore the specific enthalpy of 'damage' γ^* would be an energy of this transformation per unit volume or per unit mass. The translational resistance moment R_1 is defined as the integral of damage density over the trailing edge of the active zone[12,13]. For the case considered here, damage density is unity since transformation is homogeneous. Thus, the resistance moment R_1 is reduced to the volume of transformed material per unit crack surface created.

The specific energy of transformation γ^* is estimated from A_{1c} and R_{1c} as $\gamma^*=A_{1c}/R_{1c}$. This energy amounts to 76 MJ m^{-3}. Assuming density of transformed material to be 1.2 g cm^{-3}, $\gamma^*=15$ cal g^{-1}.

Substituting $\gamma^*=A_{1c}/R_{1c}$ in equation (1) we obtain

$$\frac{dl}{dN}=\frac{dD/dN}{A_{1c}\left(\frac{R_1(l)}{R_{1c}}-\frac{A_1(l)}{A_{1c}}\right)} \qquad (2)$$

The denominators of equations (1) and (2) express the energy barrier for active zone translation, i.e. the difference between the energy required for active zone translation γ^*R_1 and the energy available for the process A_1. Evolution of this barrier normalized by A_{1c} is shown as the shadowed area in *Figure 15*.

Stability conditions for CL translation are derived as[12]

$$\gamma^*R_1-A_1=0 \quad \text{(necessary)} \qquad (3a)$$

$$\frac{\partial(\gamma^*R_1-A_1)}{\partial l}<0 \quad \text{(sufficient if equation (3a) is met)} \qquad (3b)$$

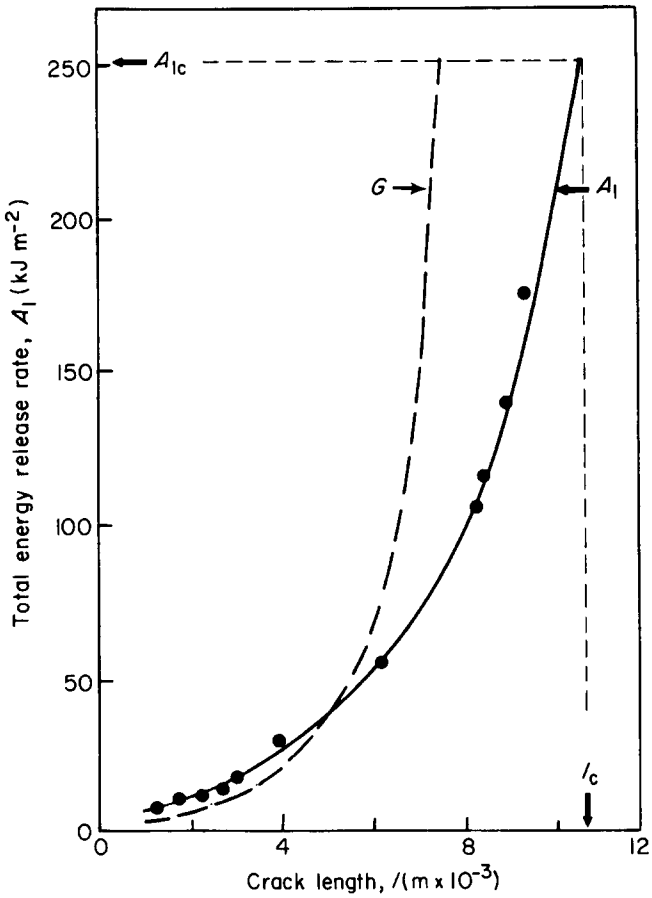

Figure 14 Comparison between the experimentally measured total energy release rate A_1 and the energy release rate G calculated using Irwin's plastic zone correction

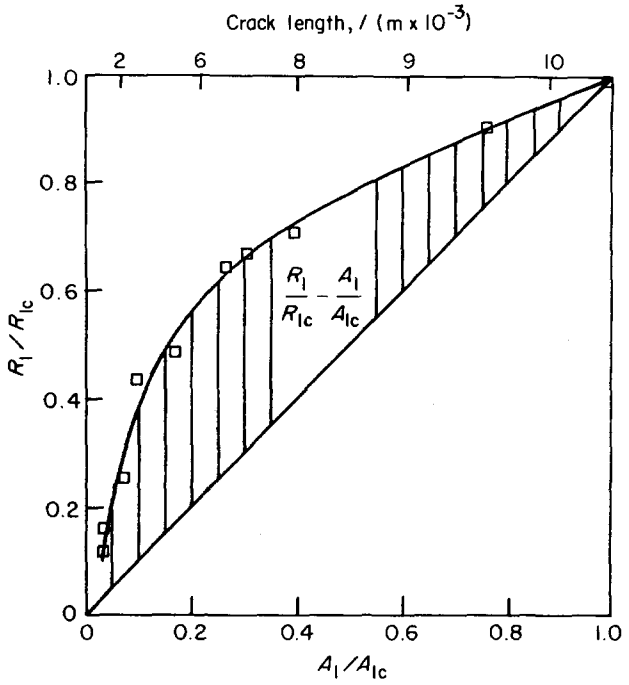

Figure 15 Evolution of the normalized resistance to CL propagation with respect to the normalized total energy release rate. The shadowed area represents evolution of the normalized energy barrier

The condition (3b) in the case considered can be rewritten as

$$A_{1c}\frac{\partial\left[\frac{R_1(l)}{R_{1c}}-\frac{A_1(l)}{A_{1c}}\right]}{\partial A_1}<0 \qquad (4)$$

i.e.

$$\frac{\partial\left(\frac{R_1(l)}{R_{1c}}\right)}{\partial\left(\frac{A_1(l)}{A_{1c}}\right)}<1 \qquad (5)$$

Thus, the condition (3b) of instability is satisfied at $A_1/A_{1c}\simeq 0.25$ (*Figure 15*). Beyond that, the condition (3a) becomes the necessary and sufficient criterion of instability.

Interesting differences in CL behaviour are observed prior to and after satisfaction of the sufficient condition (3b). For example, the crack excursion measured as discontinuous crack growth band (b) normalized by active zone length (l_a) as a function of the energy release rate (*Figure 16*) shows a definite transition at $A_1/A_{1c}\simeq 0.25$.

The active zone is commonly conceived as line plastic zone in Dugdale–Barenblatt (DB) model[9]. The plastic zone size in terms of our measurements corresponds to the active zone length l_a (*Figures 9–11*). The ratio L_a/l, according to the DB model, should be proportional to the energy release rate. The observed l_a/l vs. A_1 and Dugdale–Barenblatt model predictions are presented in *Figure 17*. The initial data points correspond to the active zone formed prior to crack initiation. If these are excluded, one notices that DB model describes the phenomenon over a limited range of A_1 which is below the condition of instability (inequality (3b)). Indeed, early analysis by Brinson[9] suggests similar limitations in ductile PC fracture. Along the same line of argument, departure of calculated G employing the Irwin's correction from measured A_1 (*Figure 14*) occurs around $A_1/A_{1c}\simeq 0.25$.

Evaluation of dissipative energy

The term dD/dN (numerator in equation (1)) expresses the energy expenditure per cycle on submicroscopic processes leading to damage formation. In general, $dD/dN=(dW_i/dN)-(dQ/dN)$, where dW_i/dN is the total work done on irreversible deformation per cycle. This can be readily obtained from the load–displacement

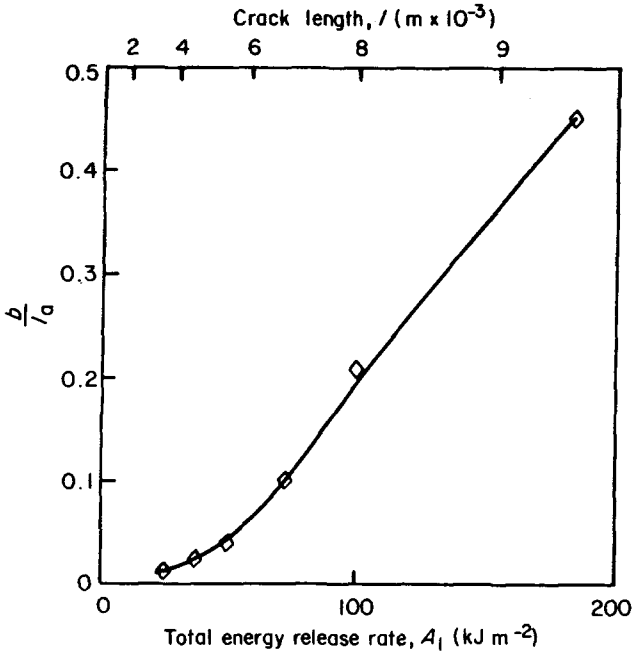

Figure 16 Discontinuous crack growth band evolution normalized by active zone length l_a during stable CL propagation

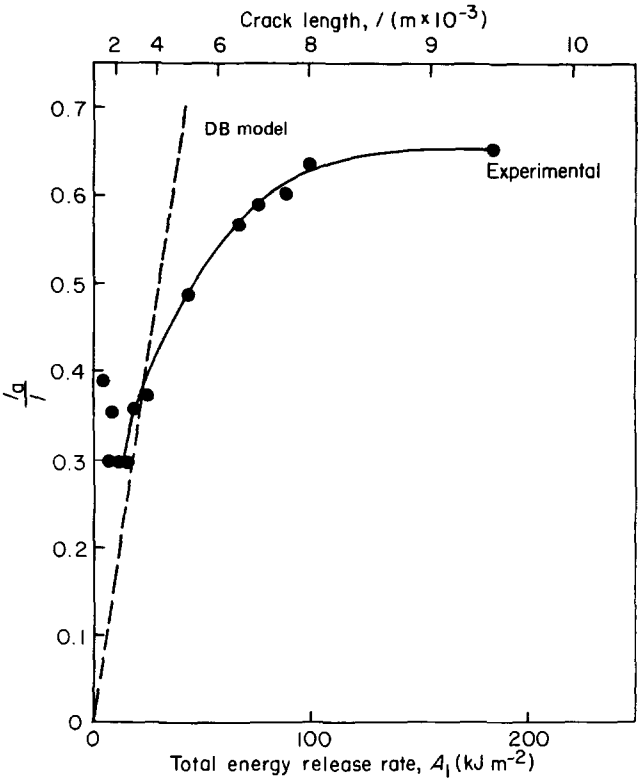

Figure 17 Experimental (l_a/l) and predicted (Dugdale–Barenblatt model) values of the plastic zone

hysteresis loops. On the other hand, dQ/dN is the amount of heat exchanged per cycle.

Heat exchange could be positive which means that a fraction of W_i is converted into heat and radiates out. This case corresponds to the conventional perception of mechanical dissipation. Alternatively, dQ/dN could be negative, i.e. the material absorbs heat from the thermostat, which assists in material transformation activated by stress concentration in the vicinity of the crack tip. Obviously, heat measurements within the active zone are necessary to resolve the issue. In absence of heat measurements, we assume $dD/dN = \beta(dW_i/dN)$ where β expresses the portion of the total irreversible work per cycle expended on damage formation. The quantity dW_i/dN is measured directly as the area of the hysteresis loop of a cracked specimen minus the area of the loop for an identical notched, yet uncracked, specimen. Evolution of the hysteresis loops during CL propagation is illustrated in *Figure 18*. The numbers at the top of each

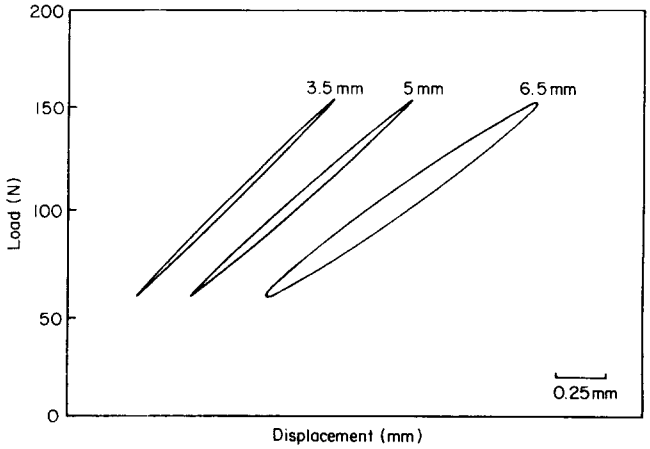

Figure 18 Representative hysteresis loops during CL propagation at selected crack lengths (3.5, 5 and 6.5 mm)

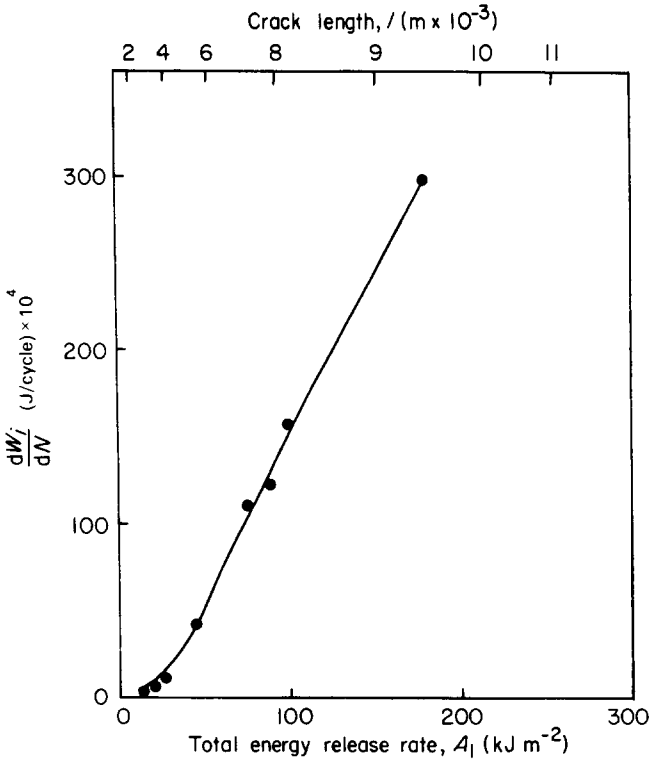

Figure 19 Irreversible work per cycle as a function of total energy release rate

loop corresponds to crack length. The irreversible work per cycle as a function of A_1 is given in *Figure 19*.

Applicability of the CL theory

All parameters of equation (2) are independently measured. The crack speed dl/dN is obtained from video recordings. The numerator of the right hand side is evaluated from hysteresis loop recordings as discussed in the previous sub-section. The denominator is evaluated from CL configuration and load–displacement measurements as described in the first sub-section of this section. The solid line in *Figure 20* is a plot of the expression

$$\frac{dW_i/dN}{A_{1c}\left(\dfrac{R_1(l)}{R_{1c}} - \dfrac{A_1(l)}{A_{1c}}\right)}$$

as a function of A_1. The data points represent dl/dN measurements. The adjustable parameter β is found to be unity. Plausibly, the heat absorbed during elastic stretching of the material compensates for the part of irreversible work dissipated as heat. The proposed formalism obviously provides a good description of the entire range of crack propagation covering more than four orders of magnitude.

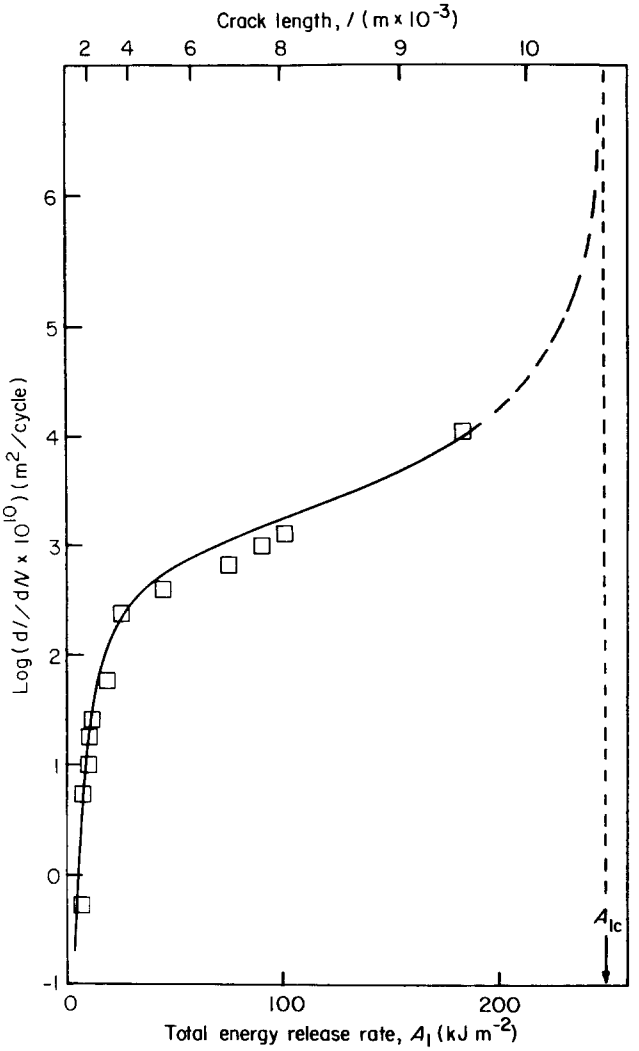

Figure 20 Crack growth rate in terms of equation (2). The data points are measurements of the left hand side and the solid line is calculated from the measured parameters of the right hand side of the same equation, with $\beta = 1$

CONCLUSIONS

(1) This paper introduces a methodology for ductile fracture propagation analysis for cases where the crack propagates preceded and surrounded by substantial amount of homogeneous material transformation.

(2) A formalism for the well known three-stage (S-shaped) fatigue crack propagation is presented in terms of material parameter γ^*, the resistence moment R_1, and the total energy release rate A_1.

(3) It is shown that the energy release rate associated with ductile FCP in polycarbonate departs markedly from that predicted by plastic zone models for well developed cracks.

(4) The specific enthalpy of transformation (yielding) for ductile PC fracture is tentatively evaluated as $\gamma^* \simeq 15\,\text{cal}\,\text{g}^{-1}$ on the basis of the conditions of CL instability.

ACKNOWLEDGEMENTS

The authors wish to acknowledge the financial support of the Dow Chemical Company and to thank Dr R. Bubeck for stimulating discussions.

REFERENCES

1 Pitman, G. L. and Ward, I. M. *Polymer* 1979, **20**, 895
2 *Idem. J. Mater. Sci.* 1980, **15**, 635
3 Hyakutake, H. and Nisitani, H. *Eng. Fracture Mechanics* 1985, **22**, 359
4 Martin, G. C. and Gerberich, W. W. *J. Mater. Sci.* 1976, **11**, 231
5 Hertzberg, R. W., Nordberg, H. and Manson, J. A. *J. Mater. Sci.* 1970, **5**, 521
6 Arad, S., Radon, J. C. and Culver, L. W. *J. Appl. Polym. Sci.* 1973, **17**, 1467
7 Parvin, M. and Williams, J. G. *Int. J. Fracture* 1975, **11**, 963
8 Andrews, E. H. and Barnes, S. R. in 'Fifth International Conference on Deformation, Yield and Fracture of Polymers', 29 March to 1 April 1982. The Plastics and Rubber Institute, Cambridge, England, pp. 8.1–8.4
9 Brinson, H. F. *Eng. Fracture Mechanics* 1985, **22**, 359
10 Donald, A. M. and Kramer, E. J. *J. Mater. Sci.* 1981, **16**, 2967
11 Kitagawa, M. *J. Mater. Sci.* 1982, **17**, 2514
12 Chudnovsky, A. 'The Crack Layer Theory', NASA Report, Case Western Reserve University, Cleveland, Ohio (1983)
13 Chudnovsky, A. and Moet, A. *J. Mater. Sci.* 1985, **20**, 630
14 Takemori, M. T. and Kambour, R. P. *J. Mater. Sci.* 1981, **16**, 1108
15 Mills, N. J. and Walker, N. *J. Mater. Sci.* 1980, **15**, 1832
16 Mackay, M. E., Teng, T. G. and Shultz, J. M. *J. Mater. Sci.* 1979, **14**, 221
17 Manson, J. A. and Hertzberg, R. W. 'Fatigue of Engineering Plastics', Academic Press, New York, 1980
18 Irwin, G. R. *Appl. Mater. Res.* 1964, **3**, 65